WILEY-VCH

DOI: 10.1002/((please add manuscript number))
Article type: Communication

Fully solution-processed photonic structures from inorganic/organic molecular hybrid materials and commodity polymers

Stefan Bachevillier, Hua-Kang Yuan, Andrew Strang, Artem Levitsky, Gitti L. Frey, Andreas Hafner, Donal D. C. Bradley, Paul N. Stavrinou, Natalie Stingelin**

S. Bachevillier, Prof. N. Stingelin
Department of Materials and Centre of Plastic Electronics, Imperial College London, London SW7 2AZ, UK

H.K. Yuan, A. Strang, Prof. P. N. Stavrinou
Department of Physics and Centre for Plastic Electronics, Blackett Laboratory, Imperial College London, London SW7 2AZ, UK

A. Levitsky, Prof. G. L. Frey
Department of Materials Science and Engineering, Technion, Israel Institute of Technology, Haifa, 32000, Israel

Dr. A. Hafner
BASF Schweiz AG, Klybeckstrasse 141, 4057 Basel, Switzerland

Prof. D. D. C. Bradley
Departments of Engineering Science and Physics, Division of Mathematical, Physical and Life Sciences, University of Oxford, Oxford, UK

Prof. P. N. Stavrinou
Department of Engineering Science, University of Oxford, Oxford, UK
E-mail: paul.stavrinou@lincoln.ox.ac.uk

Prof. N. Stingelin
School of Materials Science and Engineering and School of Chemical & Biomolecular Engineering, Georgia Institute of Technology, Atlanta, GA, USA
E-mail: natalie.stingelin@mse.gatech.edu

Keywords: solution-processed photonics, dielectric Bragg reflectors, anti-reflection coatings, inorganic/organic hybrid materials

Abstract

Managing the interference effects from multiple thin-layer structures allows for the control of optical transmittance and reflectance properties - often with very high precision. Widely used and technologically significant examples of such structures are antireflection coatings (ARCs) and distributed Bragg reflectors (DBRs), which rely on the careful control of destructive and constructive interference, respectively, between incident and reflected/transmitted radiation. While these structures have been known for over a century and have been extremely well investigated for many decades, the growing emergence of printable, large area electronics based on soluble materials brings a new emphasis. Namely the availability and use of materials in multilayer environments that are capable of transferring well-established ideas to a solution-based production. Here, we demonstrate the solution-fabrication of ARCs and all dielectric mirrors based on a DBR design utilizing alternating layers of recently developed organic/inorganic hybrid materials comprised of poly(vinyl alcohol) (PVAl), cross-linked with titanium oxide hydrates, and commercially available bulk commodity plastics. Our dip-coated ARCs exhibit an 88 % reduction in reflectance across the visible compared to uncoated glass, and fully solution-coated DBRs provide a reflection of >99 % across a 100 nm spectral band in the visible region. Detailed comparisons with transfer-matrix methods (TMM) highlight the excellent optical quality of the structures. The investigation also demonstrates the extremely low optical losses and impressive interface qualities the constituent layers exhibit. Furthermore, when exposed to elevated temperatures, the hybrid material can display a notable, reproducible and irreversible change in both the refractive index and film-thickness while maintaining excellent optical performance. In addition to allowing a degree of post-deposition tuning of the photonic structures, this may lend itself to thermo-responsive applications, including security features and product-storage environment monitoring.

Introduction

Managing the interference effects from multiple thin-layer photonic structures routinely allows for the design and control of the optical transmittance and reflectance properties of an object. With the burgeoning of soluble-semiconductor-based optoelectronic technologies, there is a growing need to seamlessly incorporate such structures with simple printing and coating methodologies that allow for large-area devices fabricated with, for example plastic-based materials and a range of solution-processable metal oxides.[1,2]

Two highly attractive one-dimensional structures in this class are antireflection coatings (ARCs) and so-called distributed Bragg reflectors (DBRs), both typically comprising all dielectric materials. Antireflection technologies are ubiquitous and enhance the performance of numerous optical products — from reading glasses, through lenses, to telescopes and solar cells.[3,4] ARCs mitigate the unwanted reflections that occur from and within the object; a situation especially important when the object itself comprises several layers of differing refractive index, e.g. a typical organic solar cell. Solution-processed ARCs have been produced for almost 60 years and have frequently been based around sol-gel chemistry.[2] While sol-gel films exhibit good uniformity, they usually require a relatively high temperature post-treatment that can limit the range of applications.[5,6]

A single-layer ARC has to fulfill the following requirement: $n_{ARC} \approx (n_{substrate})^{1/2}$, with n_{ARC} being the refractive index of the ARC coating and $n_{substrate}$ the refractive index of the substrate. This means that for low-refractive index objects (e.g. typical substrates) such as those made of glass ($n_{substrate} \approx 1.49$), the ARC coating needs a refractive index of ~1.22. This is challenging to achieve with commonly employed optical materials, unless porous structures are utilized. The latter are, however, often prone to notable light scattering effects from the air cavities leading to significant transmission losses (aerogels are generally opaque).[7,8] Moreover, many porous coatings suffer from poor mechanical properties; they are fragile and can be

difficult to produce. The constraints on refractive index are considerably lowered when multilayer ARC designs are used; a large number of layers can readily achieve impressive antireflection performance, with specific designs heavily depending on the type of application along with some consideration of the spectral bandwidth the ARC needs to operate over.[3]

Mirrors based on distributed Bragg Reflectors are another attractive class of photonic structures that can deliver a high reflection over a desired wavelength range, *e.g.*, the visible spectrum, when using suitable materials and architectures. The high wavelength selectivity is valuable for a wide range applications, such as general light management schemes in semi-transparent structures,[5,9] light in- and out-coupling structures for, respectively, photovoltaics[10,11] and organic lasers,[12–14] as well as chemical and biological sensors.[15]

As with all resonant structures, successful deployment of DBRs require precise control over the refractive indices, *n*, and thicknesses, *d*, of the constituent layers, as well as an ability to fabricate these layers with good surface and interface quality. To date, inorganic materials have often been the preferred choice for DBR fabrication. They offer a wide range of refractive indices, but typically require energy-intensive and time-consuming methodologies such as thermal evaporation, electron-beam evaporation, magnetron sputtering and ion-assisted deposition in order to deposit layers of well-defined thicknesses.[3] As a result they are frequently limited to moderate to small-area coverages; it can also be challenging to produce such structures over curved and otherwise non-planar substrates. As with ARCs, some progress has been made with solution-based-production techniques for DBRs but it is fair to say such reports are few and far between. One key limitation has been the refractive index range available for suitable soluble materials which has often not been wide enough to achieve DBRs operating over a wide spectral bandwidth. As a result, inorganic/organic hybrids have recently drawn increasing interest. In 2008, Druffel et al. produced the first polymer-based nanocomposite DBR.[16] Since then, a few groups have reported dielectric mirrors based nanocomposite materials. These produced a high reflectivity with a relatively small number of layers thanks to

an increased refractive index range that was made available. Nevertheless, these mirrors often suffered from optical losses (scattering of particles and rough interfaces), poor control of the thicknesses, or the need for long UV or temperature curing steps.[1,10,15,17–22]

Results and Discussion

We begin our investigation with ARCs, themselves a useful and well-developed example of multilayer thin-film structures.[3] While a basic ARC amounts to a single layer with an optical length of a quarter-wave, greater control over the reflectance spectrum is possible when multiple layers are incorporated. The primary requirement of any multilayer ARC is that the reflection of light from the first surface destructively interferes with reflections from subsequent interfaces; in principle, and at least at one wavelength, the net reflection can then be zero. However, for many applications, a specified low reflection is typically required over a broad spectrum, and it is meeting this stricter requirement that lies behind the many ARC designs appearing in the literature. Our interest here is to highlight, in particular, the solution-processed aspect of our structures, drawing on recently developed hybrid materials.[18] We have focused on a simple bi-layer structure[23] to significantly reduce unwanted reflection over the visible part of the spectrum (400 - 750 nm). Thereby, we took advantage of the fact that dip-coating simultaneously applies coating to both sides of a substrate. The resulting double structure greatly enhances the overall anti-reflection performance, with each bi-layer ARC, at the front and back surfaces of the substrate, acting independently (i.e. incoherently).

We aimed at bi-layer structures compring a half-wave layer of a high refractive index material ($n_{\mathrm{H}}d_{\mathrm{H}} = \lambda_0/2$) and a low-refractive index quarter-wave top layer ($n_{\mathrm{L}}d_{\mathrm{L}} = \lambda_0/4$), initially applied to both sides of the substrate (see **Figure 1a** schematic and **Table 1**). TMM modelling was used to compare the spectral reflectance from both the double bi-layer ARC sandwich structure with the single bi-layer coating (back-side layers removed after coating). In addition to the hybrid material (Figure 1a),[18] the calculations also examined equivalent bi-

layer structures based on commodity plastic polystyrene (PS; n_H = 1.59, d_H = 173 nm) and the commercially available, low-refractive index fluoropolymer poly[4,5-difluoro-2,2-bis(trifluoromethyl)-1,3-dioxole-co-tetrafluoroethylene] (PFP; n_L = 1.30, d_L = 106 nm) (Figure 1a). For such a single PS/PFP bi-layer coating, we deduce an average reflectance of around 4.5 %, while for the double bi-layer structure with a high- and a low-refractive index layer on both sides of the substrate, our calculations suggest that *R* can be reduced to less than 1 % (**Figure S1**). As shown by Table 1, a 20 vol% titanium oxide hydrates hybrid produces an equivalent optical response without the need of an annealing step. The advantage of choosing the hybrid material over PS is that it is known to crosslink upon film formation at room temperature, aiding double-layer production as it becomes insoluble when dry.[18] Crosslinking furthermore should assist with providing the structure with mechanical robustness.

Table 1. Comparison of bi-layer ARCs, using a simple two-layer top-coating architecture vs. a sandwich structure of two layers applied to both sides of the glass substrate. Calculations are carried out for the commercially available, low refractive index polymer poly[4,5-difluoro-2,2-bis(trifluoromethyl)-1,3-dioxole-co-tetrafluoroethylene] (PFP) of n = 1.30 combined either with the commodity plastic polystyrene (PS; n = 1.59) or a poly(vinyl alcohol)/20 vol% titanium oxide hydrate hybrid of comparable refractive index. The indices were measured by single film fitting and reported at λ = 550 nm. The average reflection is computed over the wavelength range from 400 to 750 nm.

	λ_0 (nm)	$n_{550\,nm}$ (-)	d (nm)	average R only top coating (%)	average R sandwich structure (%)
PFP / PS	550	1.30 / 1.59	106 / 173	4.34	0.70
PFP / Hybrid 20 vol%	550	1.30 / 1.57	106 / 175	4.32	0.66

Turning to our experimental results, the double hybrid material/PFP ARC structure performed very well over the range 400 - 750 nm, especially in comparison to pristine glass. This difference in reflectivity is visibly detectable by the naked eye, as shown by the

photographs of two glass tubes in Figure 1b (top panel), which also illustrate that the solution-processability of the materials allows for ARC production on more complex structures.

We quantified the ARCs' performances using flat sandwich structures. The reflectance spectra of hybrid materials/PFP ARCs display a reflectance <2 % between 500 - 700 nm, approaching 0 % at a wavelength of ~600 nm, compared to ~8 % for a flat, pristine glass substrate (Figure 1b, bottom panel). This is in agreement with our TMM calculations (parameters listed in **Table S1**). As expected, results from the single bi-layer coating take intermediate values, producing $R \sim 5$ % over a comparable range of wavelengths.

Having demonstrated some simple ARC structures and the utility of the solution-processing route for fabricating structures, we now examine distributed Bragg reflectors (DBRs), *i.e.* dielectric mirrors based on a large number of alternating high-*n* and low-*n* layers. As with the ARC structures, managing coherent reflections is the key to successful design, and, for the case of a DBR mirror amounts to arranging constructive interference from the interfaces within the DBR structure.[3] In arguably the most common DBR architecture, all constituent layers fulfill a quarter-wave condition at a desired Bragg wavelength, λ_0, *i.e.* the optical thicknesses are such that $n_{\mathrm{H}}d_{\mathrm{H}} = n_{\mathrm{L}}d_{\mathrm{L}} = \lambda_0/4$. In this scenario, the reflection of light from the first surface constructively interferes with reflections from subsequent interfaces leading to the desired mirror effect. This condition is partially satisfied for a range of nearby wavelengths and results in a so-called stopband, the width of which is governed by the refractive index difference, Δn, of the alternating layers and to some extent the number of periods (taking one period as one low-index and one high-index layer) making up the DBR. The number of periods forming a DBR also governs the peak reflectivity at the Bragg wavelength and several examples are illustrated in **Figure S2** for TMM modeled mirrors designed around λ_0 = 600 nm (parameters in **Table S2**). In these examples, commodity polymers such as PS and poly(methyl methacrylate) (PMMA; *e.g.* Plexiglas®), with refractive indices of 1.59 and 1.49 respectively,

provide a Δn of 0.10. Such a low Δn places a reliance on a large number of periods to reach, say, R = 100 %, but also limits the stopband width (~ 50 nm). The example in Figure S2, which does reach R = 100 %, required 40.5 periods (81 individual layers) even for this narrow wavelength range. In contrast, when Δn is increased to 0.53, calculations show that a high-R mirror can be produced with a stopband width of ~200 nm, using only 10.5 periods (21 layers). The latter can, for instance, be achieved experimentally with a PVAl/titanium oxide hydrate hybrid of 60 vol% inorganic content (n = 1.83; see SI for details) as the high refractive index material and PFP as the low-n component.

Drawing on our numerical investigations, DBRs comprising PFP and a PVAl/titanium oxide hydrate hybrid with a 60 vol% inorganic content, were fabricated on glass substrates using a dip-coating deposition method in air at room temperature. Our initial target center wavelength was λ_0 = 730 nm; accordingly, a 10.5-period structure requiring individual layer thicknesses of 135 and 110 nm for the high- and the low-refractive index layer, respectively, was produced.

The measured transmittance spectrum of the fully solution-processed DBR is shown in **Figure 2a** (red trace) together with the TMM fitting, displayed as dotted lines (see **Table S3** for details). A few, immediate observations can be made: i) The maximum reflection of the DBR reaches 98 % at 730 nm and the overall spectrum matches very well with that calculated from the TMM suggesting that the sequential deposition of 21 individual layers was performed with excellent control and reproducibility and that the extracted refractive indices for the layers are accurate. ii) Sharp, well-defined and increasing amplitude interference fringes appear next to the stop-band region, as expected for DBRs of high uniformity, and their appearance here allow us to further highlight the reproducibility of deposition, not only for individual layers but also multiple periods of these layers. iii) The high transmittance regions outside the stopband additionally emphasize the quality of the DBR as any defects or irregularities within the layers

or at the interfaces there-between would tend to lead to unwanted light scattering and a lower transmittance.

Having established that both ARCs and multi-period DBRs of high quality can be produced from solution, we explored whether we can exploit the fact that the refractive index and film thickness of PVAl/titanium hydrate hybrid materials can change, reproducibly and irreversibly, upon exposure to elevated temperatures to produce, for instance, responsive structures.[18]

For this, we first established the extent to which the *n* and *d* of hybrid thin-films change during heat exposure. We started by measuring the transmittance and reflectance on PVAl/titanium oxide hydrate hybrid films on glass (**Figure 3a**). Because of the refractive index difference between the hybrid material and glass substrate, clear Fabry-Perot oscillations can be observed for every hybrid composition, highlighting the excellent film quality that can be obtained. The optical quality of the hybrid material likely originates from its amorphous nature, where the presence of the polyol PVAl seems to limit the formation of nanoparticles/aggregates of titanium oxide.[18] Indeed, no crystalline particles are detected even using high-resolution transmission electron microscopy (**Figure S3**), consistent with the absence of light scattering. The transmittance and reflectance spectra of the hybrid films are mirror images of each other at wavelengths above 400 nm, that is $R + T \sim 100$ % (Figure 3a), further emphasizing the very low optical loss for these materials.

To quantify the changes in refractive index and film thickness due to heating we turn to the Fabry-Perot oscillations, evident in any transmission or reflection spectra from sufficiently thick, high-quality films (**Figure S4**). Upon heating, the oscillations blue shift in comparison to those from an unheated film, suggesting the optical length of the film (*nd*) has increased; the amplitude of the oscillations also increases, entirely consistent with an increase in refractive index. Through recursive fitting, the calculated TMM spectra are compared with experimental spectra, and as there are no optical losses, we can straightforwardly extract both the refractive

index and thickness of the single hybrid layers over a range of compositions and temperatures. Cauchy parameters for wavelength-dependent refractive indices are listed in **Table S4**. Ellipsometric analysis on films deposited on silicon substrates confirms the suitability of the Cauchy form to describe the hybrid material (**Figure S5**). Thus, master curves for *n*, *d* and *nd* with temperature can be determined, shown in Figure 3c for a hybrid material comprising 60 vol% titanium oxide hydrates.

Since the titanium oxide hydrates and PVAl absorb only in the UV, any breakdown and/or degradation of the polymer or loss of inorganic species would primarily impact this part of the spectrum. To ensure this does not occur upon annealing, we assessed the absolute loss of intensity, absorptance $A = 100\ \% - R - T$. We used absorptance because volume-, or thickness-, dependent measurements probe total material content. The overall material content, thus, should remain constant if the fraction of constituent species is unchanged, but any significant loss of titanium or polymer degradation would cause variations in *A*. This would be difficult to determine from a thickness-independent property, such as absorption**,** because an increase in refractive index –due to greater dispersion– will lead to a more pronounced absorption, as stated by the Kramers-Kronig relations.[24]

Reassuringly, upon annealing the hybrid material, we find no change in its absorptance (**Figure S6** and **Figure S7**). From this observation, we conclude that annealing is not detrimentally affecting the titanium oxide hydrates and/or the PVAl matrix. It is also important to highlight that they hybrid material can be fully annealed such that its optical properties is not affected anymore when exposing it to another heat treatment step.

With confirmation of material stability to annealing, the *nd* curves may be applied such a post-deposition treatment to tune the optical response from produced multilayer structures. For instance, a DBR response might be spectrally fine-tuned to a desired wavelength range via annealing; or the design of an ARC may be adjusted to ensure that appropriate account is taken of subsequent process steps in a device fabrication. As an example, we return here to the 10.5-

period 'as-cast' mirror displayed in Figure 2a, with an initial center wavelength of λ_0 = 730 nm (Note: the optical response of the 'as-cast' mirror was taken a few hours after the fabrication, while the "aged" mirror, corresponds to the data point at 25 ˚C of Figure 2b),where further condensation reactions and physical contraction had taken place during storage at ambient conditions).

We now recall that for the as-cast device, n_H = 1.66, d_H = 135 nm, n_L = 1.30 and d_L = 110 nm, thus, $n_H d_H / \lambda_0$ = 0.31, $n_L d_L / \lambda_0$ = 0.20. The as-cast structure is slightly off a quarter-wave condition yet exposing it to a temperature of 130 °C should result (according to Figure 3c) in a stack with layers of n_H = 1.80, d_H = 88 nm, n_L = 1.30 and d_L = 110 nm , *i.e.*, $n_H d_H / \lambda_0$ = 0.26 and $n_L d_L / \lambda_0$ = 0.24, hence bringing the structure closer to the quarter-wave condition for a Bragg wavelength around 600 nm. Figure 2a displays the measured transmittance spectrum from the annealed structure which clearly shows that the expected performance, based on the master curves, is achieved. While the high-index hybrid layers uniformly shrink upon heating, with an attendant change of refractive index, the low- refractive-index layers (PFP) do not, as may be expected for a fluoropolymer. In this scenario, heating an entire DBR mirror in a single step allows us to tune its response from the near infrared ($\lambda_0 \approx$ 730 nm) to the visible ($\lambda_0 \approx$ 600 nm), resulting in an evident change in reflective color from transparent to yellow/orange. Bringing the structure closer to the quarter-wave condition and simultaneously raising Δn, increases the DBR's reflection (yielding $R \approx$ 100 %) and the width of its stopband (yielding FWHM ≈ 150 nm). The measured reflectance and calculated absorptance can be found in **Figure S8**. An optical loss <2 % is observed within the optical stop-band which is remarkably low for a solution-processed DBR. These observations are all in very good agreement with the TMM calculations. Further evidence for the high quality of the mirror produced through annealing is provided by comparison of the phase from modeling with that extracted from the reflectance spectra using a Weiner-Lee algorithm.[25,26] Here the good agreement, particularly

the linear response within the reflectance band, is characteristic of a uniformly repeated modulation of refractive index (Figure 2a).

Given the ease with which these DBRs (and ARCs) can be produced from solutions, potentially using conventional coating and printing techniques, it is perhaps worth noting that the thermal response from these photonic structures could find use in thermo-responsive indicators, heat labels (*e.g.*, for food products, perfumes, and electronic components) and, generally, applications that require monitoring of the temperature to which they are exposed. We also note that extracting the phase is extremely useful in identifying the Bragg wavelength from DBRs, especially those with a low number of periods where tracking the center of an (often asymmetric) stopband can be ambiguous. The phase difference of reflected rays at the Bragg wavelength is zero for phase modulo π. This occurs at the center of the longest slope in phase, corresponding to the DBR stop band. Recording the transmittance spectra for intermediate annealing temperatures and extracting the phase spectrum allowed us to show the expected blue-shift of the Bragg wavelength as a function of annealing temperature, as illustrated in Figure 2b.

3. Conclusions

We have demonstrated fully solution-processed high-quality antireflection coatings and dielectric mirrors fabricated at room temperature. These are constructed using high-index novel organic/inorganic hybrid materials based on the bulk commodity plastic poly(vinyl alcohol) and TiO_2-precursors such as titanium tetrachloride, in combination with a low-index fluoropolymer (PFP). It is important to note that non-chlorinated precursors, including titanium isopropoxide, can be used instead of the titanium tetrachloride. The hybrid materials enable straightforward solution-deposition and highly reproducible film formation, and offer accurate and beneficial post-deposition tuning of film properties, including refractive index *n* and layer thickness *d*. The dip-coated ARCs were shown to reduce the reflectance from glass by close to

90% when using a simple bi-layer design, while also DBRs of pronounced and well-defined stopbands could be produced using this deposition method. The high quality of the dielectric mirrors (DBRs) was deduced, among other things, by the observation of sharp oscillations in the transmittance spectra and the high transmittance achieved outside the stopband. Moreover, thanks to the large contrast in refractive indices between the two materials, a broad stopband of 150 nm and a reflection > 99 % at the Bragg wavelength can be achieved using only 10.5 periods (21 layers). The specific materials and solution processed fabrication of the structures disclosed here should be helpful to advance the further development of low-cost and large-area photonic structures, including thermo-responsive devices such as heat sensors and labels.

4. Experimental Section

Materials: Titanium(IV) chloride ReagentPlus® (purity > 99.9 %), Poly(vinyl alcohol) (PVAl) Mowiol® 18-88 ($M_w \approx 130$ kg·mol^{-1}; residual content of acetyl groups = 10.0 - 11.6 %), poly[4,5-difluoro-2,2-bis(trifluoromethyl)-1,3-dioxole-co-tetrafluoroethylene] (PFP) AF 2400 (dioxole 87 mol%) and perfluorodecalin (95 %) were purchased from Sigma-Aldrich.

Single film preparation: Stock solutions of titanium oxide hydrates of 1 or 2 M, depending on the final viscosity needed, were initially hydrolyzed as previously described.[18] Hybrid solutions of various inorganic-organic ratios were prepared by introducing corresponding amounts of $TiCl_4$ hydrolyzed solution to a 40 g·L^{-1} aqueous solution of PVAl under stirring at room temperature. Volume fractions were calculated as previously reported.[18] For single films, solutions were spin-coated on glass or quartz substrates with speeds between 800 and 5000 rpm and dry in air at room temperature.

Fabrication of ARCs and DBRs: Multilayer samples were fabricated by dip-coating of glass substrates in air at ambient temperature. Owing to the crosslinking of the hybrid films, alternation of dipping in hybrid solutions (formulated from 1 M titanium oxide hydrate

solutions and 20 g·L^{-1} PVAl aqueous solution) and PFP solution in perfluorodecalin (100 mg/mL) was possible. Withdrawal speeds were varied between 5 and 30 mm/min in order to achieve the precise thickness required for the optical quality layers. Between each layer, samples were left to dry vertically inside the fume hood for at least 20 minutes before the next layer. After few hours of drying in air at room temperature and atmospheric pressure, the sample is considered as 'as-cast'. Further ageing for ~2 days, the sample stabilizes and is considered 'aged' at 25 ˚C. A final annealing was performed once all the layers were deposited and dried. Annealing was carried out in an oven for 5 minutes in air and atmospheric pressure.

Surface profilometry: Thickness of samples were measured using a Dektak 3 surface profilometer as a function of withdrawing speeds in order to establish calibration curves. Thicknesses were in good agreement with values extracted using transfer-matrix method on transmittance spectra.

UV-Visible spectroscopy: Total transmittance of thin-films and multilayer structures were measured at normal incidence using a double-beam Shimadzu UV-2600 spectrophotometer equipped with an integrating sphere. Total reflectance was measured with the same instrument at an incident angle of 8°, allowing the specular reflectance to be captured by the sphere. A spectral range between 220 to 1400 nm was accessible. Reconstructing the phase from experimental spectra involved forming a sine series from the cosine series resulting from the Fourier transform of reflection amplitude. This is possible owing to the fact that reflection and phase form real and imaginary parts of a complex function,[25] thus their corresponding fourier transforms are even and odd respectively. The algorithm was implemented utilizing a Wiener-Lee transformation.[26]

Optical modeling: Coherent transmittance and reflectance were calculated using the Fresnel coefficient form of the TMM.[3] Complex refractive index and thicknesses of the hybrid were used as inputs to the code. Since the substrates used were of thicknesses much greater than the wavelength of light, 1 to 2 mm, an incoherent contribution was also included.[3] When fitting

experimental data, the TMM model was used as an objective function with refractive index and thickness as fitting parameters. The MATLAB Levenberg-Marquardt algorithm[27,28] was implemented to minimize the TMM model chi-squared value until a local minimum was found. Fitting results were cross-checked with thicknesses from profilometry, expected refractive indices as well as visual inspection of functional overlap. To reduce the number of free parameters at one time, substrate indices were fit first in the absence of any sample film. Furthermore, long wavelength regions of spectra (e.g. above 550 nm) were fit first without refractive index dispersion (i.e. $n_b = 0$). With n_a determined, n_b was fit by including short wavelengths. Only non-absorbing wavelengths above 400 nm were included, eliminating the imaginary part of refractive index.

Ellipsometry: A J.A. Woollam variable-angle spectroscopic ellipsometer was used to guide and confirm results from TMM fitting.

Supporting Information

Supporting Information is available from the Wiley Online Library or from the author.

Acknowledgements

The authors SB and HKY contributed equally to this work. SB, HKY, PS, DDCB and NS thank the UK's Engineering and Physical Sciences Research Council (EPSRC) for funding via the Centre for Doctoral Training in Plastic Electronics Materials, PE-CDT (EP/G037515/1). SB, HKY, DDCB, PS and NS furthermore acknowledge funding provided by BASF Schweiz AG towards this PE-CDT project. NS, PS and GF are, moreover, grateful for support by the Marie Skłodowska-Curie Actions Innovative Training Network "H2020-MSCAITN-2014 INFORM – 675867". NS and GF in addition acknowledge support by the United States-Israel Binational Science Foundation (BSF), Jerusalem, Israel.

Received: ((will be filled in by the editorial staff))
Revised: ((will be filled in by the editorial staff))
Published online: ((will be filled in by the editorial staff))

References

[1] D. Comoretto, *Organic and Hybrid Photonic Crystals*, Springer, 2015.

[2] H. Dislich, P. Hinz, *Journal of Non-Crystalline Solids* 1982, *48*, 11.

[3] H. A. Macleod, *Thin-Film Optical Filters, Third Edition*, CRC Press, 2001.

[4] H. K. Raut, V. A. Ganesh, A. S. Nair, S. Ramakrishna, *Energy & Environmental Science* 2011, *4*, 3779.

[5] H. Dislich, E. Hussmann, *Thin Solid Films* 1981, *77*, 129.

[6] D. Chen, *Solar Energy Materials and Solar Cells* 2001, *68*, 313.

[7] J.-Q. Xi, M. F. Schubert, J. K. Kim, E. F. Schubert, M. Chen, S.-Y. Lin, W. Liu, J. A. Smart, *Nature Photonics* 2007, *1*, 176.

[8] Y.-F. Huang, S. Chattopadhyay, Y.-J. Jen, C.-Y. Peng, T.-A. Liu, Y.-K. Hsu, C.-L. Pan, H.-C. Lo, C.-H. Hsu, Y.-H. Chang, C.-S. Lee, K.-H. Chen, L.-C. Chen, *Nature Nanotechnology* 2007, *2*, 770.

[9] M. E. Calvo, J. R. Castro Smirnov, H. Míguez, *J. Polym. Sci. B Polym. Phys.* 2012, *50*, 945.

[10] C. Bronnbauer, J. Hornich, N. Gasparini, F. Guo, B. Hartmeier, N. A. Luechinger, C. Pflaum, C. J. Brabec, K. Forberich, *Advanced Optical Materials* 2015, *3*, 1424.

[11] J. R. C. Smirnov, M. E. Calvo, H. Míguez, *Advanced Functional Materials* 2013, *23*, 2805.

[12] L. M. Goldenberg, V. Lisinetskii, S. Schrader, *Laser Phys. Lett.* 2013, *10*, 055808.

[13] G. Canazza, F. Scotognella, G. Lanzani, S. D. Silvestri, M. Zavelani-Rossi, D. Comoretto, *Laser Phys. Lett.* 2014, *11*, 035804.

[14] L. M. Goldenberg, V. Lisinetskii, S. Schrader, *Appl. Phys. B* 2015, *120*, 271.

[15] Z. Wang, J. Zhang, J. Li, J. Xie, Y. Li, S. Liang, Z. Tian, C. Li, Z. Wang, T. Wang, H. Zhang, B. Yang, *J. Mater. Chem.* 2011, *21*, 1264.

[16] T. Druffel, N. Mandzy, M. Sunkara, E. A. Grulke, *Small* 2008, *4*, 459.

[17] M. E. Calvo, O. S. Sobrado, G. Lozano, H. Míguez, *J. Mater. Chem.* 2009, *19*, 3144.

[18] M. Russo, M. Campoy-Quiles, P. Lacharmoise, T. A. M. Ferenczi, M. Garriga, W. R. Caseri, N. Stingelin, *Journal of Polymer Science Part B: Polymer Physics* 2012, *50*, 65.

[19] Z. Wang, J. Zhang, J. Xie, Y. Yin, Z. Wang, H. Shen, Y. Li, J. Li, S. Liang, L. Cui, L. Zhang, H. Zhang, B. Yang, *ACS Appl. Mater. Interfaces* 2012, *4*, 1397.

[20] T. Ogata, R. Yagi, N. Nakamura, Y. Kuwahara, S. Kurihara, *ACS Appl. Mater. Interfaces* 2012, *4*, 3769.

[21] I. R. Howell, C. Li, N. S. Colella, K. Ito, J. J. Watkins, *ACS Appl. Mater. Interfaces* 2015, *7*, 3641.

[22] C. Bronnbauer, A. Riecke, M. Adler, J. Hornich, G. Schunk, C. J. Brabec, K. Forberich, *Advanced Optical Materials* 2017, *6*, 1700518.

[23] L. A. Catalán, *J. Opt. Soc. Am., JOSA* 1962, *52*, 437.

[24] V. Lucarini, J. J. Saarinen, K.-E. Peiponen, E. M. Vartiainen, *Kramers-Kronig Relations in Optical Materials Research*, Springer-Verlag, Berlin Heidelberg, 2005.

[25] A. Papoulis, *The Fourier Integral and Its Applications*, McGraw-Hill, New York, NY, 1962.

[26] A. Carballar, M. A. Muriel, *Journal of Lightwave Technology* 1997, *15*, 1314.

[27] K. Levenberg, *Quarterly of applied mathematics* 1944, *2*, 164.

[28] D. W. Marquardt, *Journal of the society for Industrial and Applied Mathematics* 1963, *11*, 431.

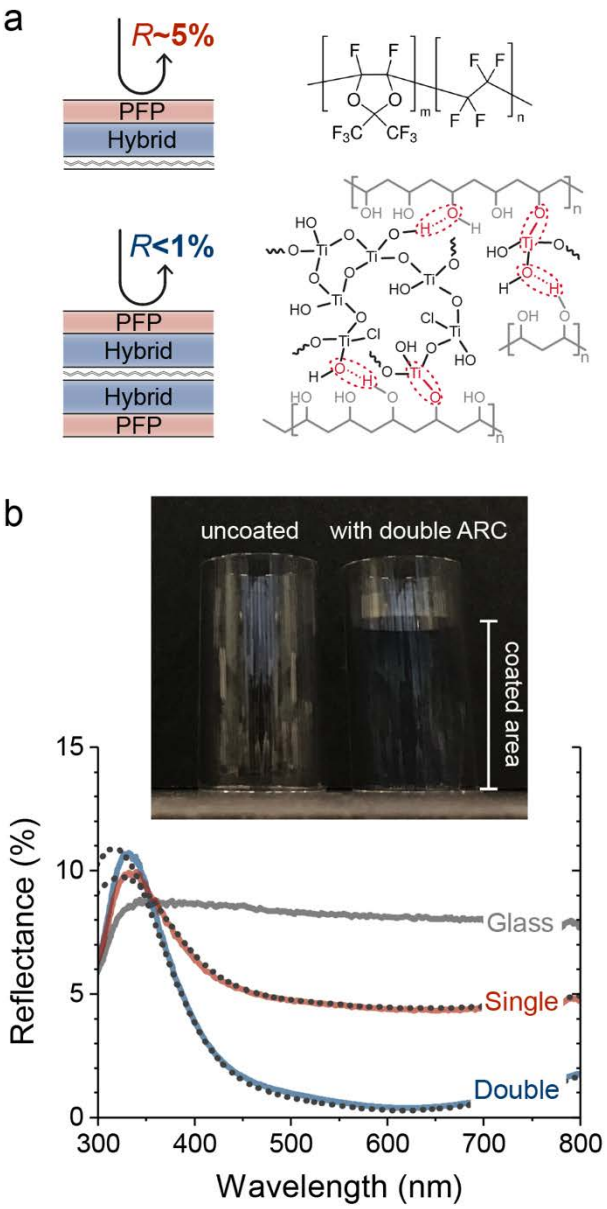

Figure 1. a) Schematics of bi-layer and sandwiched bi-layer ARC architectures (left panel) and chemical structures of low index fluorinated polymer poly[4,5-difluoro-2,2-bis(trifluoromethyl)-1,3-dioxole-co-tetrafluoroethylene] and crosslinked poly(vinyl alcohol)/ titanium oxide hydrate hybrid (right panel). This renders the hybrid insoluble yet highly transparent, even with high loadings of inorganic components. b) Reflectance spectra of the ARC coating on a flat glass substrate resulting in an 88 % drop in reflectance across the visible. The TMM calculated reflectance spectra (black dotted lines) agree well with the experimentally obtained data (solid curves) confirming the control of the deposition system and materials processing. The photograph shows a pristine tube substrate, taking advantage of the solution-process, without coating and one with the dip-coated sandwich ARC structure.

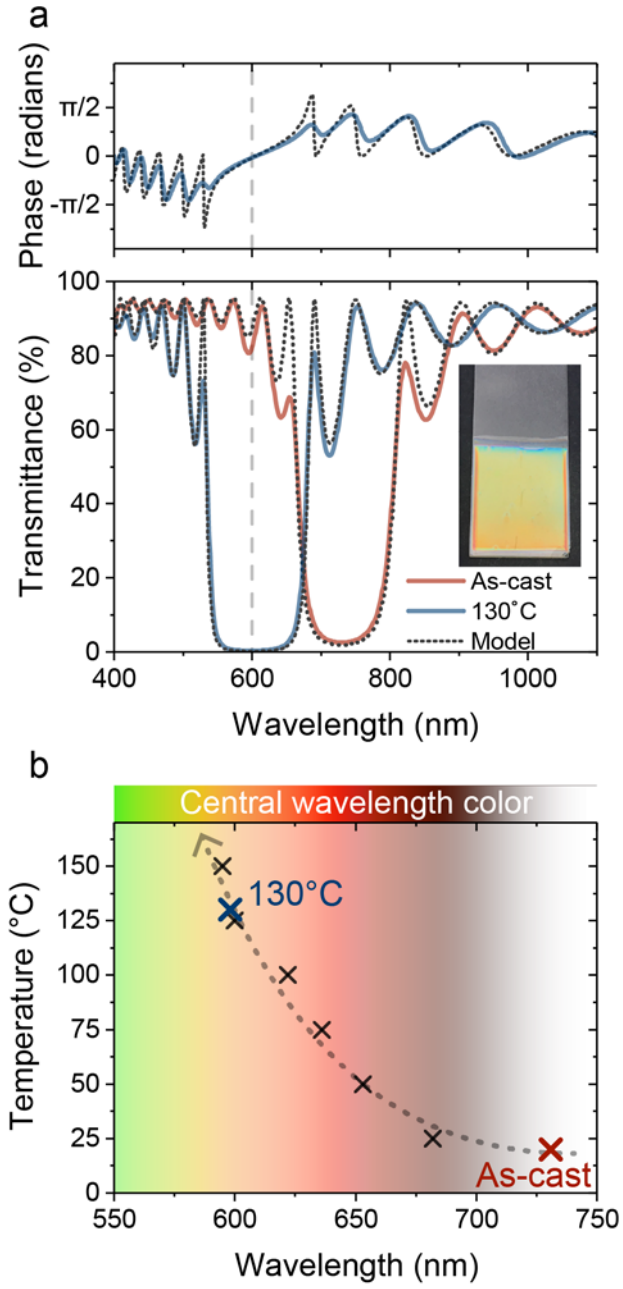

Figure 2. Tunable 10.5-period distributed Bragg reflector processed from 60 vol% titanium hybrid and the fluorinated polymer PFP on a glass substrate. a) Bottom: Transmittance spectra of the as-cast and annealed at 130 ˚C DBRs. The blue-shift of the reflectance band was pre-designed to account for the large contraction of the hybrid layers during annealing, allowing for the benefits of an increased refractive index, primarily a wider and deeper reflectance-band. TMM modeling (black dotted lines) of the structure before and after annealing confirm the repeatability of the deposition and the accuracy of refractive indices for the hybrid system. The inset shows an example of a dip-coated DBR. Top: Comparison of modeled DBR reflectance phase with that extracted from experimental. b) The Bragg wavelength of the DBR device tracked as a function of annealing temperature. Experimental crosses are determined from zero-crossing spectral positions of the transmitted phase, the dotted line is a guide for the eye showing the progressive displacement of the center wavelength with temperature.

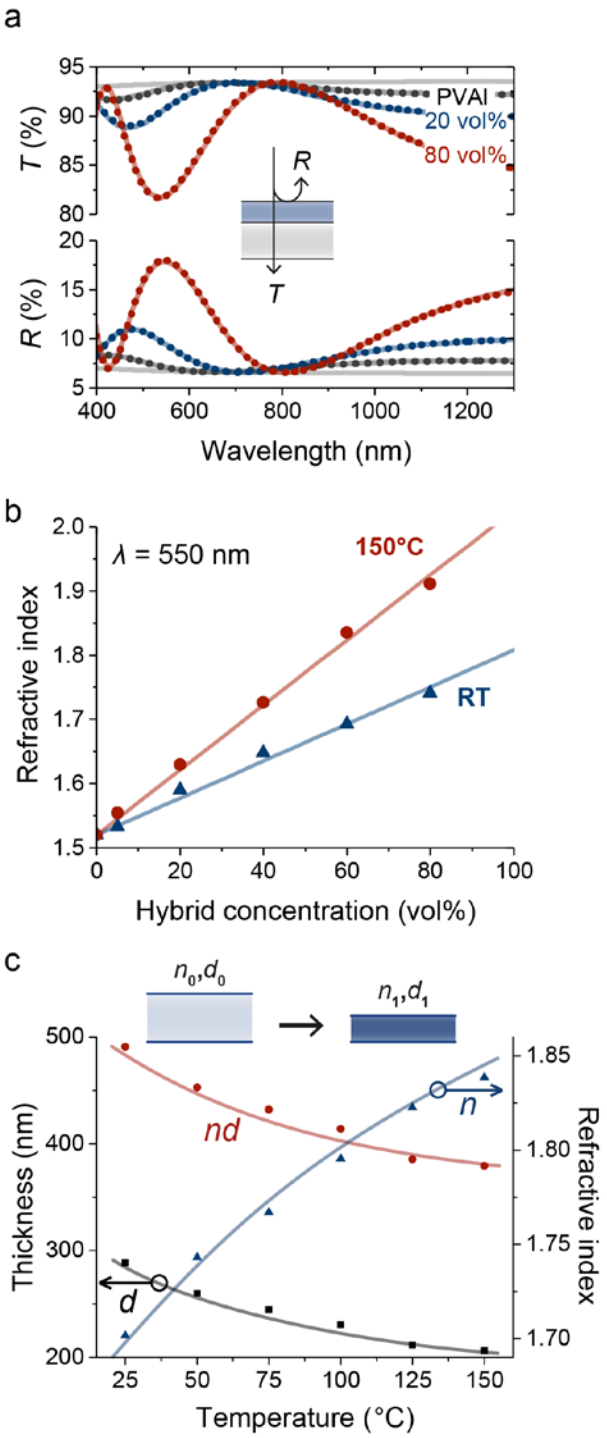

Figure 3. a) Transmittance and reflectance spectra of 0, 20 and 80 vol% titanium hybrid films, all deposited to a thickness of 220 nm on quartz substrates. *R* and *T* are mirroring each other, indicating very little loss of intensity due to absorption. The low optical losses are confirmed by the TMM modeling of the spectra (dotted line) that assumes zero loss, and qualitatively by the coincidence of the transmission maxima with that of the bare substrate. b) Refractive index at wavelength 550 nm of hybrid films at different concentrations (0, 20, 40, 60 and 80 vol%). A refractive index range of almost 0.5 without optical losses is readily accessible using different organic/inorganic ratios and annealing temperature. Values were extracted by the TMM modeling of transmittance spectra. c) Thickness and refractive index of a 60 vol% hybrid film as a function of annealing temperature. Both values guided by TMM fitting. Inset shows hybrid film which experiences further condensation with temperature.

Table of contents

Fully printed ARC and DBRs with a reflection <1 % over the visible range and, respectively, >99 % across a 150 nm wide reflectance band, are demonstrated. With the use of a tunable inorganic/polymer hybrid, the DBR is thermo-responsive with a stop-band blue-shifting by 150 nm with temperature. The development of printable high-quality photonic structures is an enabling step for low-cost and large area applications.

Keyword: solution-processed photonics, dielectric Bragg reflectors, anti-reflection coatings, inorganic/organic hybrid materials

Stefan Bachevillier, Hua-Kang Yuan, Andrew Strang, Artem Levitsky, Gitti L. Frey, Andreas Hafner, Donal D. C. Bradley, Paul N. Stavrinou, Natalie Stingelin**

Title: Fully solution-processed photonic structures from inorganic/organic molecular hybrid materials and commodity polymers

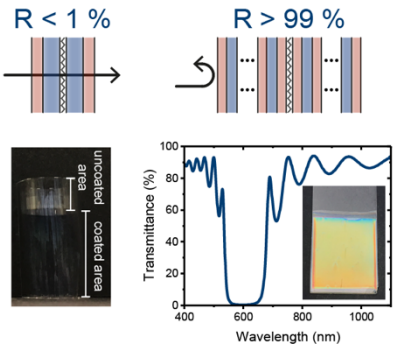

Supporting Information

Fully solution-processed photonic structures from inorganic/organic molecular hybrid materials and commodity polymers

Stefan Bachevillier, Hua-Kang Yuan, Andrew Strang, Artem Levitsky, Gitti L. Frey, Andreas Hafner, Donal D. C. Bradley, Paul N. Stavrinou, Natalie Stingelin**

Titanium oxide hydrate/PVAl hybrid:

Inorganic/organic hybrids can be tuned by changing the ratio of both components. The most straightforward unit to express the hybrid concentration is the number of titanium atoms per gram of polymer, expressed as mol Ti/g PVAl. However, it was measured by Russo et al. that a simpler scale can be followed using volume percentage.[17] It can be calculated by using **Equation S1**. 20 vol% and 60 vol% titanium hybrids correspond to 4.3 and 25.8 mmol Ti/g PVAl.

$$vol\%\ Ti = \frac{V_{Ti\ species}}{V_{Ti\ species}+V_{PVAl}} \times 100 = \frac{{}^{(n_{Ti\ species}\cdot M_{Ti\ species})}/_{\rho_{Ti\ species}}}{{}^{(n_{Ti\ species}\cdot M_{Ti\ species})}/_{\rho_{Ti\ species}}+V_{PVAl}} \times 100 \qquad \text{(S1)}$$

with $M_{Ti\ species}$ = 90 g·mol^{-1} and $\rho_{Ti\ species}$ = 1.95 kg·m^{-3}

More details can be found in reference.[18]

Anti-reflection coatings:

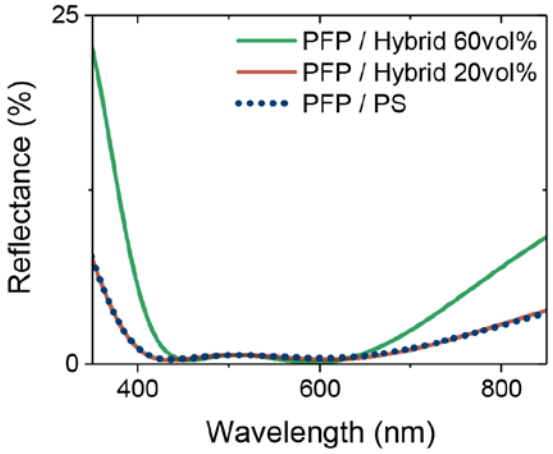

Figure S1. Calculated reflectance from double bi-layer ARCs with PFP and polystyrene (PS) or two different hybrids. Optical responses are very similar when a hybrid with 20 vol% of titanium oxide hydrates or PS are used. Reflection increases on the edges of the visible range when high index 60 vol% hybrid is used with PFP.

Table S1. Parameters deduced for a solution-processed bi-layer sandwich ARC (see Figure 1c for structure) based on high-refractive index layers produced from PVAl/20 vol% titanium oxide hydrate hybrid and low-refractive index PFP layers. Thicknesses and refractive indices were extracted from TMM modeling. The resulting nd / λ_0 values are close to the required quarter-wave *resp.* half-wave coating conditions (given in brackets).

Single ARC	λ_0 (nm)	n_{550nm} (-)	d (nm)	nd / λ_0 (-)
Hybrid 20 vol%	550	1.57	169	0.49 (0.50)
PFP	550	1.30	116	0.27 (0.25)
Double ARC	λ_0 (nm)	n_{550nm} (-)	d (nm)	nd / λ_0 (-)
Hybrid 20 vol%	550	1.57	166	0.47 (0.50)
PFP	550	1.30	112	0.26 (0.25)

Distributed-Bragg Reflectors:

Following **Equation S2**, a higher number of layers increases the reflectance as shown in Figure S2. A higher refractive index contrast between the low and high index layers allows the widening of the stopband but also the reduction the number of periods necessary to achieve high reflectivity (Table S3 and Figure S2).

$$R_N = \left[\frac{1-(n_H/n_L)^{2N}}{1+(n_H/n_L)^{2N}}\right]^2 \quad \text{(S2)}$$

Table S2. Calculated optical responses of PMMA/PS DBRs and PFP/hybrid 60 vol% DBRs. Large index contrasts reduce the number of periods necessary and widen the stop-band.

	λ_0 (nm)	n_{600nm} (-)	Number of periods (-)	FWHM (nm)	Max Reflectance (%)
PMMA / PS	600	1.49 / 1.59	10.5	54	49
PMMA / PS	600	1.49 / 1.59	40.5	30	98
PFP / PS	600	1.30 / 1.59	10.5	105	96
PFP / Hybrid 60 vol%	600	1.30 / 1.83	10.5	151	99.8

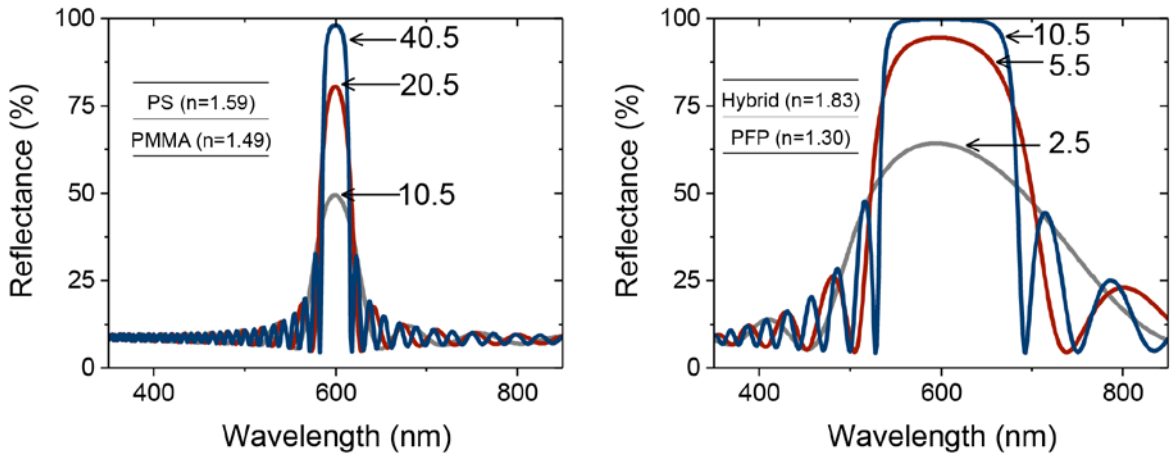

Figure S2. Calculated reflectance from DBRs with a low index contrast (left panel) and a larger index contrast (right panel). The numbers by the spectra indicate the number of periods used. A larger refractive index contrast is seen to broaden the reflectance band and sharply increase the reflectance from an equivalent number of layers- this is clear by comparing the spectra for 10.5 period structures.

Table S3. Parameters used for the DBR shown in Figure 2a, as-cast and after annealing at 130°C. Thicknesses were extracted from TMM modeling for the 60 vol% hybrid and PFP thin films assuming no variation in thickness between each period. Refractive indices used in the modeling were characterized previously. Measured nd / λ_0 values are close to the ideal case shown in brackets after annealing, resulting in high reflectivity. For the as-cast situation, values are slightly off-set, as anticipated. They correspond to the as-cast parameters leading to the tuned device at λ_0 = 600 nm after annealing. PFP layers did not change with annealing. Precise calibration was required to precisely predict the change in refractive index and thickness for the hybrid layers.

As-cast	λ_0 (nm)	n_{730nm} (-)	d (nm)	nd / λ_0 (-)
60 vol% hybrid	730	1.66	135	0.31 (0.25)
PFP	730	1.30	110	0.20 (0.25)
130°C	λ_0 (nm)	n_{600nm} (-)	d (nm)	nd / λ_0 (-)
60 vol% hybrid	600	1.80	88	0.26 (0.25)
PFP	600	1.30	110	0.24 (0.25)

Titanium oxide hydrate/PVAl hybrid characterization:

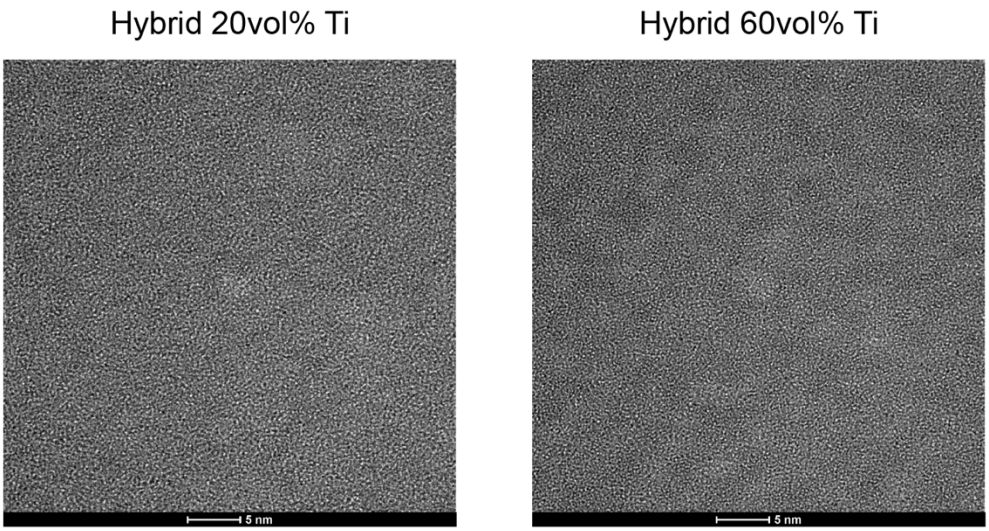

Figure S3. Cross-sectional high-resolution transmission electron microscopy of dip-coated hybrid films with 20 vol% and 60 vol% titanium oxide hydrates. The absence of fringes confirms the fully amorphous structure of the hybrid.

Fitting of refractive index:

A Cauchy dispersion relation was used for the real part of refractive index *n* in order to fit the measured Fabry-Perot oscillations with the TMM,

$$\boldsymbol{n(\lambda) = n_a + n_b/\lambda^2} \quad \textbf{(S3)}$$

where n_a is a wavelength independent constant and n_b (μm^{-2}) describes the index dispersion. The Cauchy coefficients for the wavelength-dependent refractive index that we deduce at different temperatures and hybrid compositions are listed in Table S4 which were in good agreement with ellipsometry data obtained on such film between 400 to 1400 nm (Figure S5).

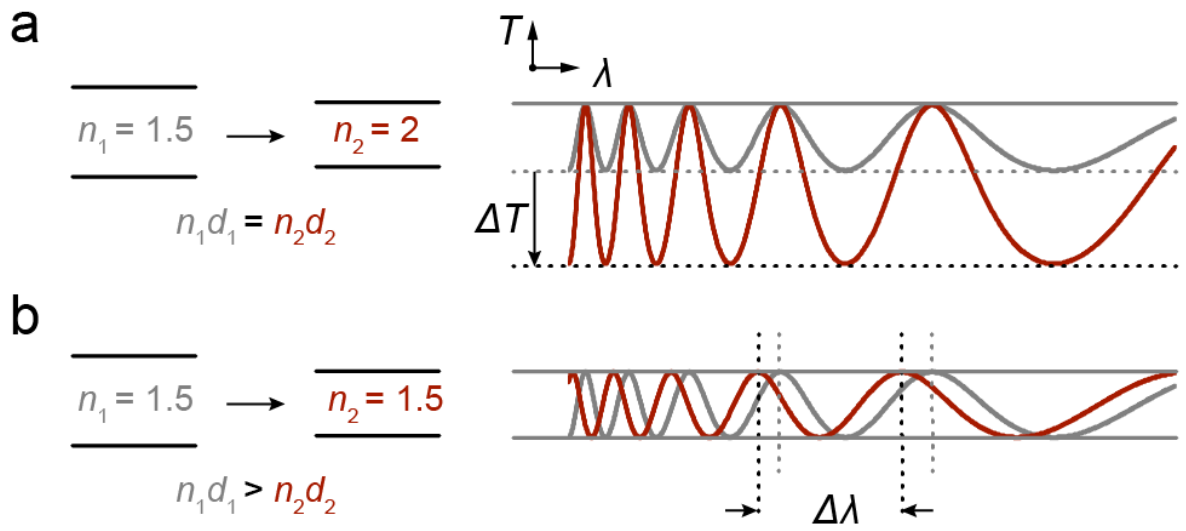

Figure S4. Transmittance spectra highlighting the effect of refractive index, *n*, and thickness, *d*, on both the amplitude and period of interference oscillations. a) Increasing *n* increases the depth of oscillation. Maintaining equal optical thickness, *nd*, ensures interference extrema remain at the same wavelengths. b) Conversely decreasing *d* whilst maintaining *n*, such that *nd* decreases, causes red-shifting of interference extrema. In addition, the period between extrema reduces. The lack of change in amplitude confirms its exclusive dependence on *n*.

Table S4. Cauchy parameters for wavelength-dependent refractive index of PVAl/titanium oxide hydrate hybrids for different titanium oxide hydrate composition after annealing at 25, 100 and 150 ˚C (n_b in units of μm^{-2}).

Inorganic content in PVAl/titanium oxide hydrate hybrid	20 vol%	40 vol%	60 vol%	80 vol%
25 ˚C	$n_a = 1.57$ $n_b = 0.006$	$n_a = 1.62$ $n_b = 0.012$	$n_a = 1.65$ $n_b = 0.016$	$n_a = 1.68$ $n_b = 0.022$
100 ˚C	$n_a = 1.58$ $n_b = 0.009$	$n_a = 1.66$ $n_b = 0.013$	$n_a = 1.72$ $n_b = 0.025$	$n_a = 1.75$ $n_b = 0.025$
150 ˚C	$n_a = 1.59$ $n_b = 0.010$	$n_a = 1.68$ $n_b = 0.014$	$n_a = 1.75$ $n_b = 0.029$	$n_a = 1.82$ $n_b = 0.032$

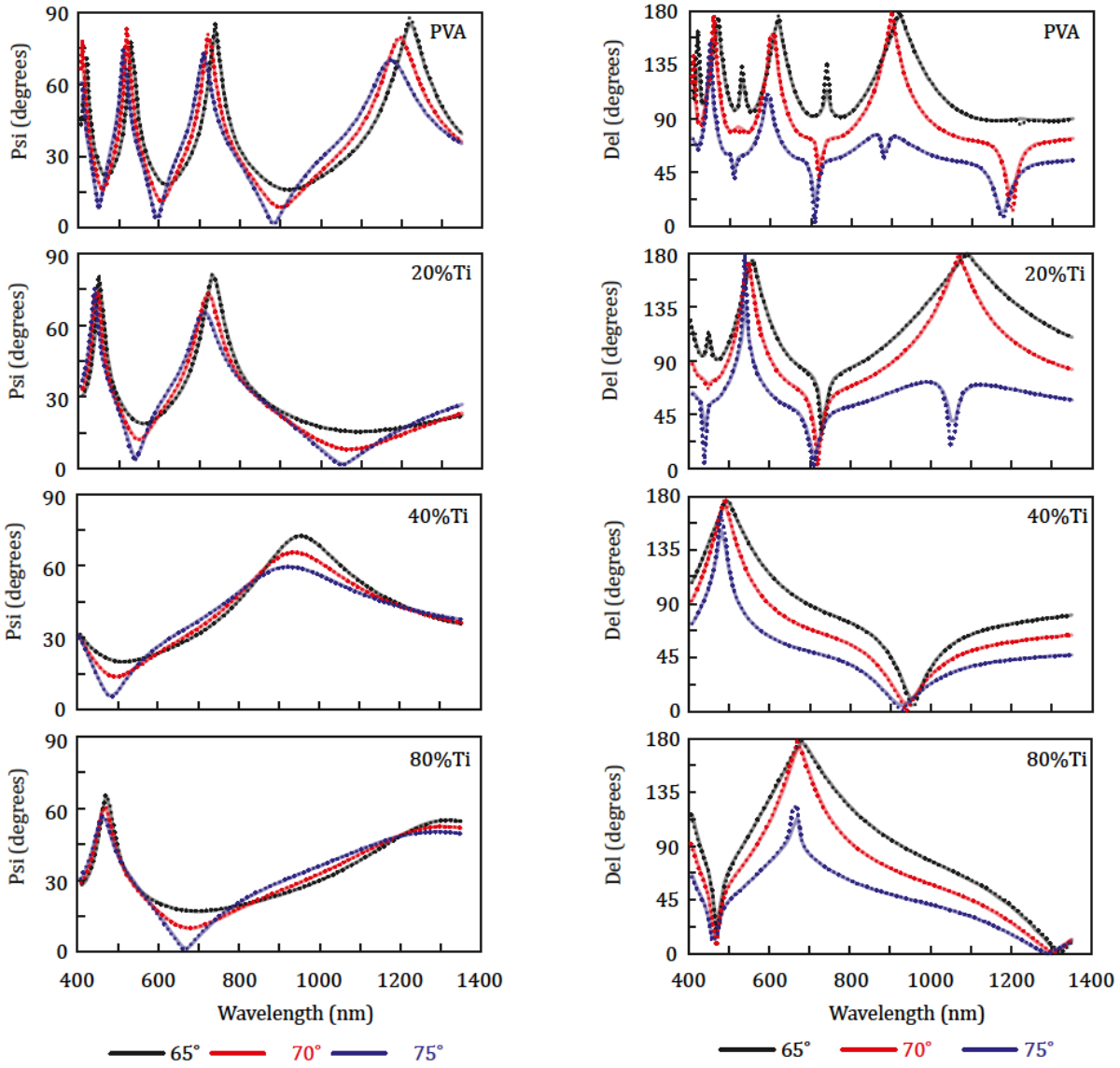

Figure S5. Measured and calculated plots of Psi and Delta for PVA, 20, 40 and 80 vol% PVAl/titanium oxide hydrate hybrid films spin-coated onto a silicon wafer. The agreement between measured and calculated spectra is excellent across the entire wavelength range, suggesting that the Cauchy description for the extracted index is highly suitable.

Thermal stability of hybrid:

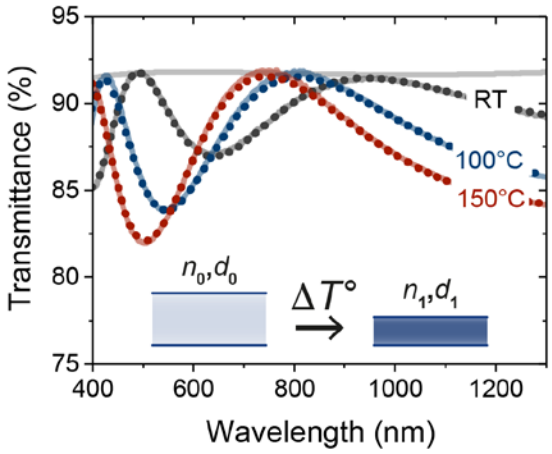

Figure S6. Transmittance of 60 vol% titanium hybrid film deposited on glass before and after annealing at 100 ˚C and 150 ˚C. Low losses are demonstrated by the TMM modeling of the spectra (dotted line) with $k = 0$, and qualitatively by the coincidence of the transmission maxima with that of the bare substrate. Inset shows a hybrid film that experience further condensation with temperature. It induces a contraction of the film up to 30 % without cracking, and an increase in refractive index.

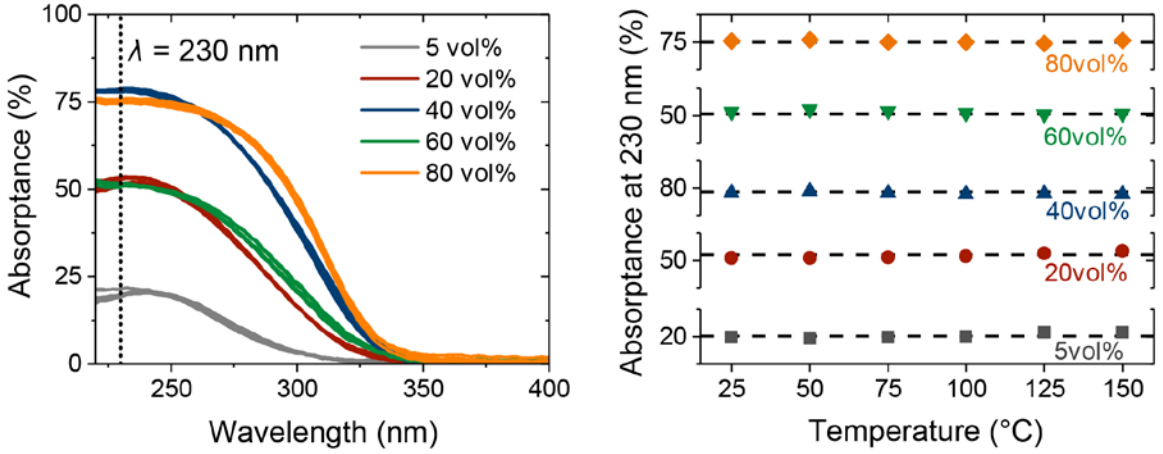

Figure S7. Left: Superposition of absorptance of hybrid films before and after annealing at 50, 75, 100, 125 and 150 ˚C. Absorptance is calculated after measuring total transmittance and reflectance using $A = 1 - T - R$. Maximum absorptance is at wavelength around 230 nm corresponding to absorption band of titanium oxide. Right: Absorptance at 230 nm after each annealing is constant. It indicates that no titanium is leaving the film during annealing. Furthermore, the constant shape of the absorptance curves as a function of wavelength confirms the absence of any degradation happening during the condensation process, for example the deterioration of the polymer.

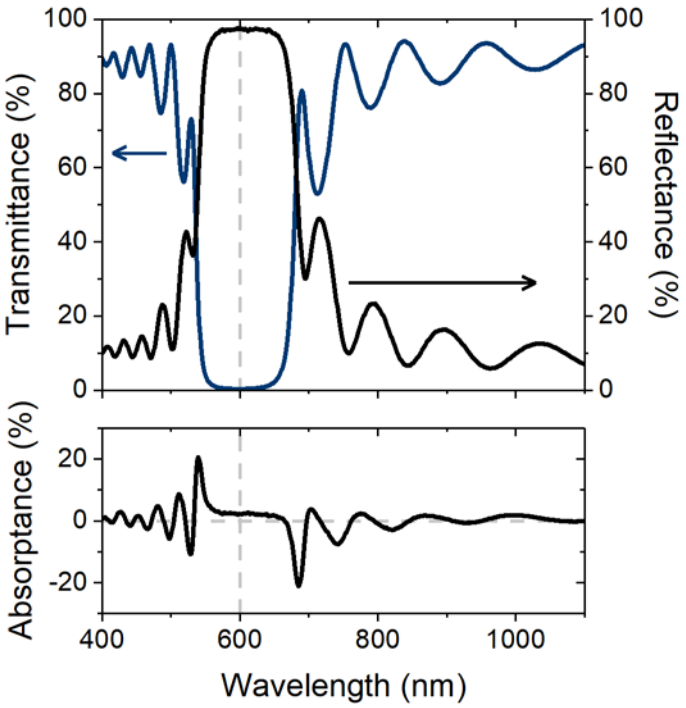

Figure S8. Measured transmittance and reflectance (top panel) along with calculated absorptance spectra (bottom panel) of the 10.5-period DBR discussed in Figure 2. It was processed from 60vol% titanium hybrid and PFP followed by an annealing at 140 ˚C. The reflectance was taken at an incident angle 8˚.